

Approximate Air-Fluid Interactions for SPH

Christoph Gissler^{1,2} Stefan Band¹ Andreas Peer¹ Markus Ihmsen² Matthias Teschner¹

¹University of Freiburg, Germany

²FIFTY2 Technology GmbH

Abstract

Computing the forces acting from a surrounding air phase onto an SPH free-surface fluid is challenging. For full multiphase simulations the computational overhead is significant and stability issues due to the high density ratio may arise. In contrast, the air-fluid interactions can be approximated efficiently by employing a drag equation. Here, for plausible effects, the parameterization is important but challenging. We present an approach to calculate the parameters of the used drag equation in a physically motivated way. We approximate the deformation and occlusion of particles to determine their drag coefficient and exposed surface area. The resulting effects are validated by comparing them to the results of a multiphase SPH simulation. We further show the practicality of our approach by combining it with different types of SPH solvers and by simulating multiple, complex scenes.

Categories and Subject Descriptors (according to ACM CCS): I.3.7 [Computer Graphics]: Three-Dimensional Graphics and Realism—Animation

Keywords: physically-based animation, fluid simulation, Smoothed Particle Hydrodynamics, multiphase

1. Introduction

Since air is normally invisible, liquids tend to look like single-phase, free-surface flows. It is intuitive to assume that liquids like water do not interact with any other phase, as these interactions are often not directly visible. However, the surrounding air influences the behavior of liquids significantly. Rain drops, for example, reach a terminal velocity or otherwise they would hurt a lot.

Although the interactions of liquids with their surrounding air are important, in the Computer Graphics community, single-phase approaches are often preferred. One of the main reasons is that a single-phase liquid simulation is computationally cheaper. Of the two major approaches used to simulate fluids, the Eulerian and the Lagrangian one, the Lagrangian approach is especially well-suited to simulate free-surface, single-phase flows. This is due to its meshless discretization of the fluid volume with moving sample points, which implicitly track the fluid surface. The Lagrangian Smoothed Particle Hydrodynamics (SPH) method is a popular choice (cf. [IOS*14]) which we also use in this work.

In the context of SPH, there exist multiple approaches to capture the effects coming from the interaction between the simulated liquid and the surrounding air. Fully simulating the air phase is possible and logically allows to capture all occurring effects. However, the computation of such multiphase simulations is very expensive since a large volume needs to be sampled with air particles to enclose the liquid. Furthermore, stability problems may occur due to the high density ratio between air and liquid.

To prevent the cost of simulating the air phase, approaches have been implemented that try to reproduce the observed interaction effects without the need for a fully simulated second phase. Some approaches sample air particles only in regions of interest [SB12] to capture the behavior of bubbles [MSKG05, IBAT11] or spray and foam [IAAT12]. These approaches require careful placement and deletion strategies for the air particles and do not model the effects of air acting as a drag force on the surface of the liquid. Simple drag forces are already employed in particle-based fluid simulations, for example in [MMCK14]. Accurate parameter estimation is normally not done.

Contribution. We present an approach to model drag forces acting from an air phase with predefined velocities onto a free-surface SPH fluid. We employ the drag equation to compute one-way coupled forces acting onto the fluid surface. We calculate the surface of each fluid particle and additionally model its deformation to accurately estimate the parameters needed to compute the drag force.

Using the drag equation to model the drag forces has several advantages. It means that the forces are mainly based on the velocity difference between air and fluid. Since we do not compute explicit pressure values for the interaction between the phases, typical instabilities that occur due to high density ratios are prevented. Furthermore, we do not need to sample the air with particles, which reduces the computational cost of the simulation.

Our approach produces results that are similar to a full multiphase simulation (see Fig. 1). We also simulate realistic scenar-

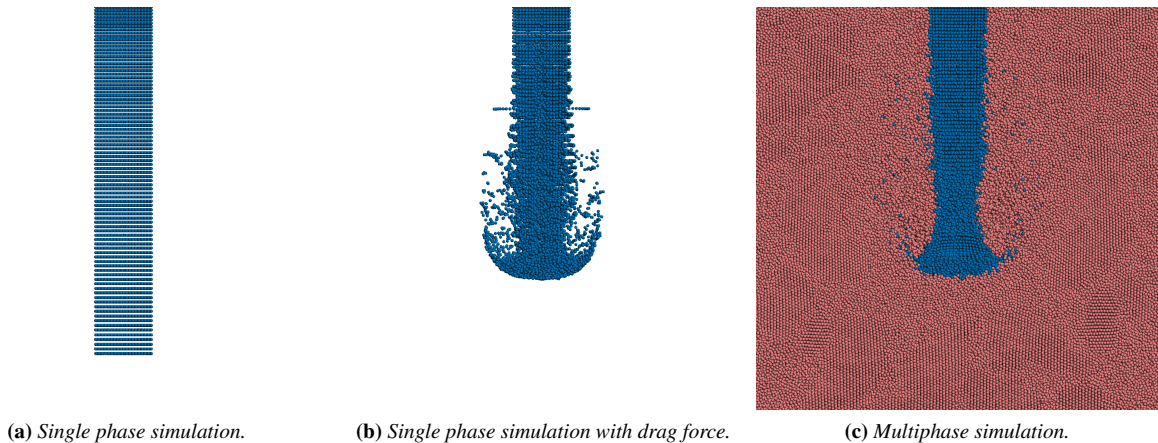


Figure 1: Comparison of a single phase simulation without drag force, one with our proposed drag force and a multiphase simulation. Employing our drag force yields a similar result as the multiphase simulation.

ios which show that employing our proposed drag force improves the plausibility of the fluid behavior (see Figs. 2 and 7). The proposed drag force can be combined with different types of SPH fluid solvers, which we also demonstrate.

Since we do not explicitly sample the air with particles, our approach is unable to reproduce effects coming from entrapped air like rising air bubbles. Furthermore, as the air is not simulated and the force is only one-way coupled, we cannot model effects based on the fluid influencing the air.

Organization. In the next section, we will first discuss related work regarding SPH and fluid-air coupling in more detail. Then, in Section 3, a short introduction to SPH fluid solvers is given with an overview over the different types of possible solvers for the Navier-Stokes equation. In Section 4, we present our method to model the air effects acting on the fluid. This section includes an explanation of the drag equation and detailed sections how we model the droplet deformation and compute the surface area of a particle. In Section 5, we show simulations employing our proposed force. We demonstrate the improvements when using our model by comparing it to simulations without it and to a full multiphase simulation. Finally, we summarize our work and give suggestions for future work in Section 6.

2. Related Work

For the simulation of single-phase, free surface liquids, SPH was first introduced to the Computer Graphics community by Müller et al. [MCG03]. Since then, a lot of research has been done to improve the performance and extend the possible effects that can be simulated with SPH. There exist multiple overviews regarding SPH [Mon05] and its use for fluid simulation [IOS*14].

There exist extensions for SPH to simulate multiple phases and their interaction. In the Computer Graphics community, Müller et al. [MSKG05] stress the importance of modeling the interaction between a liquid phase and the surrounding air and first proposed an SPH multiphase formulation. However, due to density

discontinuities across the interface, spurious tension effects and large gaps occur between phases. Replacing the usage of density in the SPH formulation with the number density reduces this problem [TM05, SP08]. Nevertheless, using a full multiphase simulation to model the effects between air and liquid is challenging. For a multiphase simulation, a large domain surrounding the liquid has to be sampled with air particles. This is computationally expensive. Furthermore, the high density ratio between air and liquid leads to high accelerations of the air phase. To get a stable simulation, small time steps are needed. Additionally, as detailed in [SP08, LSRS99], SPH particles order themselves in stable lattice structures. This damps the buoyancy of single particles submerged inside another phase [IBAT11].

Instead of fully simulating the second phase, approaches exist that only generate air particles in regions of interest. Most of the work deals with simulating entrapped air bubbles. For example, in [MSKG05], air particles are generated at the liquid-air interface and deleted if they do not interact with liquid anymore. The interactions between the air and liquid particles are computed with a multiphase SPH model. When the air particles are generated, their velocity is set to the velocity of the surrounding liquid particles. This means that no strong pressure or friction forces occur between the phases. Due to stability problems, [MSKG05] increases the density of air particles to reduce the density ratio between the phases. Additionally, they introduce an artificial buoyancy force such that the entrapped air particles behave plausible. Similarly, Ihmsen et al. [IBAT11] generate air particles on the fly to model bubbles. Instead of using a multiphase SPH model like in [MSKG05], all interaction forces are computed based on velocity differences between the phases. This brings improvements when dealing with high density ratios. Similarly, our approach also only relies on the velocity difference between the phases to compute the interaction forces. One of the coupling forces used in [IBAT11] is a drag force. It scales linearly in the velocity difference and is used to model friction forces between the phases. Rising bubbles are also modeled in [CPPK07, HLYK08]. Here, a drag force is used to couple the

bubbles with the surrounding liquid, too. Both the Stokes law and the drag equation are used in [CPPK07] to compute the drag force based on the Reynolds number of the bubble. In contrast to our work, in [CPPK07], the drag coefficient needed for the drag equation is set to a constant value and the deformation of single particles is not modeled. In [SB12], similar to [MSKG05], air particles are only generated near the liquid-air interface. However, in [SB12], this is not done to model entrapped air. Instead, the air particles are used to improve the SPH density estimation of particles at the surface of the fluid. No pressure or viscosity forces are evaluated between the phases. In contrast to the aforementioned approaches, which either improve the density estimation or model entrapped air, our approach tries to model the drag effects of air acting on a liquid's surface. Also, our approach does not generate any air particles. Our used drag equation is similar to the one in [CPPK07]. We do, however, take special care to compute the drag coefficient and to model particle deformation.

Drag forces acting from the air onto the surface of another material are often used in animation to improve cloth simulations. Bhat et al. [BTH*03] combine a linear relationship between velocity differences and forces for tangential areas and a quadratic one for areas exposed in normal direction to the air. They state that the quadratic term is needed in order to capture more realistic effects. Wilson et al. [WMLS14] also use a drag equation to model the effects of air on clothes. In their work, the drag coefficient is controlled by the artist using the simulation tool. In their unified, position-based simulation framework [MMCK14], Müller et al. also model drag effects on clothes. They employ the aerodynamic forces proposed in [KKTW04]. Furthermore, they use a simple drag force to model the interaction of air with smoke, which is discretized with particles. As a condition when to apply the drag force they use a simple density-based approach, assuming that surface particles have a lower density than internal particles. Their drag force is linear in the velocity difference, modeling friction forces. In order to scale the effect of the force, they use a user-defined parameter. In contrast to their work, our approach is designed to compute air forces acting on a liquid instead of smoke. We use a drag term that is quadratic in the velocity difference and we take special care to automatically compute all necessary parameters in order to keep user input to a minimum.

3. SPH-based Fluid Solver

A common approach for SPH-based fluid solvers is to solve the Navier-Stokes equation in order to compute an acceleration for each fluid particle i :

$$\frac{D\mathbf{v}_i}{Dt} = -\frac{1}{\rho_i} \nabla p_i + \nu \nabla^2 \mathbf{v}_i + \frac{\mathbf{F}_i^{\text{external}}}{m_i}. \quad (1)$$

SPH is used to discretize the spatial derivatives in Eq. (1). In order to calculate these derivatives, SPH requires the neighboring particles of each particle.

To compute the pressure gradient and – following – the acceleration due to pressure, the pressure value must be computed for all particles. The pressure acceleration should prevent compression of the fluid. Accordingly, the pressure depends on the density, which is also computed using SPH. Using this density, the pressure can

be calculated using an equation of state (EOS) as it is done, for example, for WCSPH [BT07]. Iterative EOS solvers allow to use larger time steps [SP09, BK17]. Finally, a splitting scheme can be employed, leading to a pressure Poisson equation (PPE). The PPE is solved to get the pressure value. IISPH [ICS*14] is an example for this type of pressure solver.

There are also several possibilities for evaluating the acceleration due to viscosity. One way is to compute it explicitly. In this case, there exist various options for discretizing the Laplacian with SPH. In [MFZ97], for example, a combination of a finite difference and the kernel gradient is used to improve its robustness with regard to particle disorder. Alternatively, the viscosity acceleration can also be solved using an implicit scheme, examples are [TDF*15, PICT15, BK17].

Finally, Eq. (1) contains the external forces $\mathbf{F}_i^{\text{external}}$ which – for example – consist of the gravity. We add our proposed drag force to these external forces. This allows us to easily integrate our force into different types of SPH solvers.

4. Air interactions

We want to model the forces acting from the surrounding air onto a free-surface liquid. These interactions are defined by pressure, friction and adhesion forces. We do not model the effects of adhesion as it can be approximated by adjusting the surface tension parameters of the liquid. For low relative velocities between air and liquid, drag effects can be modeled using a linear relationship between the relative velocity and the acting forces. The corresponding formula is called the Stokes' law. For higher velocities, a quadratic relationship between relative velocity and force is needed. We focus on modeling the drag effects using this quadratic relationship. The drag equation is a general formula to model these forces acting on an object i moving through the air [And01]:

$$\mathbf{F}_i^{\text{drag}} = \frac{1}{2} \rho_a \mathbf{v}_{i,\text{rel}}^2 C_{D,i} A_i. \quad (2)$$

ρ_a is the density of the air. $\mathbf{v}_{i,\text{rel}}^2$ is a vector pointing in the direction of the relative velocity difference between air and the object i , while its length is given as the squared length of this velocity difference. It is computed as follows:

$$\mathbf{v}_{i,\text{rel}}^2 = |\mathbf{v}_a - \mathbf{v}_i|^2 \frac{\mathbf{v}_a - \mathbf{v}_i}{|\mathbf{v}_a - \mathbf{v}_i|} = |\mathbf{v}_a - \mathbf{v}_i| (\mathbf{v}_a - \mathbf{v}_i).$$

\mathbf{v}_i is the velocity of particle i and \mathbf{v}_a is the air velocity. In our work, the air velocity is predefined for every position in space. The drag coefficient $C_{D,i}$ and the exposed cross-sectional area A_i vary for each object. They allow to tune the model for differently shaped objects.

Eq. (2) is normally used to compute the aerodynamic drag of rigid objects such as airplanes or cars. It builds upon the dynamic pressure $q = \frac{1}{2} \rho |\mathbf{v}|^2$ and models the molecules of the air phase hitting the object and being stopped in the process. When assuming that all air molecules come to a complete stop when hitting the surface, the drag coefficient $C_{D,i}$ should be chosen as 1. Depending on the shape of the surface, however, not all molecules of the air come to a stop. Accordingly, the drag coefficient varies depending on the shape of the considered object.

Due to its general nature, the drag equation can also be used to compute the drag force acting onto a liquid like water. As an additional complexity compared to rigid objects, a liquid changes its shape continuously. To compute the drag forces acting on an SPH liquid, we compute Eq. (2) independently for each particle. Accordingly, we need to estimate their drag coefficient $C_{D,i}$ and their exposed cross-sectional surface area A_i .

A single particle is the smallest discretized element in an SPH simulation. To more accurately estimate the surface area, we additionally model the deformation of particles. This deformation influences the drag coefficient as well as the cross-sectional area of a particle. To explain the different parts leading to the final computation of Eq. (2), this section is structured as follows: First, as the other parts depend on it, we explain how we model the deformation of a particle. Then, in Subsection 4.2, we use this deformation to compute the drag coefficient for each particle. The exposed cross-sectional area of a particle depends on two parts. First, the unoccluded area of the particle in the direction of the air, explained in Subsection 4.3, and second, the occlusion of a particle by other liquid particles or a rigid boundary. We present our occlusion computation method in Subsection 4.4. Finally, in Subsection 4.5, we summarize the subsections and combine all formulas to compute the drag force acting on a particle.

4.1. Particle Deformation

We want to compute the deformation of a fluid particle due to the drag forces from the surrounding air. If a droplet consists of multiple SPH particles, its overall deformation is represented by the position of the particles with respect to each other. Therefore, we consider every particle on its own and do not try to change or model the overall structure of multiple fluid particles that are clustered together.

Theory. To model the deformation of a particle, we follow the Taylor-Analogy-Breakup (TAB) model that was initially proposed in [OA87] to model engine spray droplet breakup. A fluid droplet in the air oscillates with time t [NG72, VM12]. The TAB model is based on the Taylor analogy [Tay63] which relates this oscillation to a mass-spring system. In [OA87], the deformation of a droplet is described by the formula of a damped harmonic oscillator. The external force, the spring force and the damping force are dependent on the phase of the droplet and the surrounding air phase. Constants C_F , C_d and C_b are introduced to scale these external, spring and damping forces. An additional constant C_b is used to convert the displacement to a dimensionless deformation y_i . This current deformation y_i of a particle i is then a value between 0 and 1. A value of 0 means there is no deformation (droplet is a sphere) and a value of 1 corresponds to a deformed droplet (droplet is a disk). Accordingly, in [OA87], the change of y_i over time is described by the following second order ordinary differential equation:

$$\frac{d^2 y_i}{dt^2} = \frac{C_F}{C_b} \frac{\rho_a}{\rho_l} \frac{v_{i,rel}^2}{L^2} - \frac{C_k \sigma}{\rho_l L^3} y_i - \frac{C_d \mu_l}{\rho_l L^2} \frac{dy_i}{dt}. \quad (3)$$

ρ_a and ρ_l are the rest densities of the air and the liquid. σ is the surface tension coefficient of the liquid and μ_l is the dynamic viscosity of the liquid. By default, we set these values according to literature to $\rho_a = 1.2041$, $\rho_l = 1000$, $\sigma = 0.0724$ and $\mu_l = 0.00102$. For the

constants C_F , C_k and C_d , we adopt the values proposed in [OA87] which are $C_F = \frac{1}{3}$, $C_k = 8$, $C_d = 5$. C_b is set to $\frac{1}{2}$. Finally, L is the radius of the droplet. Since we consider each particle on its own, we take the radius of a sphere corresponding to the volume h^3 of a particle. It is calculated as:

$$h^3 = \frac{4}{3} \pi L^3 \\ \Leftrightarrow L = \sqrt[3]{\frac{3}{4\pi} h^3}.$$

Implementation. It is possible to compute the deformation of a particle over time by applying numerical integration to Eq. (3). This would require to additionally store the current deformation per particle. To prevent this memory overhead and to simplify the implementation, we make simplifying assumptions. First, we follow [OA87] and assume a constant relative velocity to find the solution to Eq. (3) which reads:

$$y_i(t) = \frac{C_F}{C_k C_b} We_i + e^{-\frac{t}{t_d}} \left(\left(y_0 - \frac{C_F}{C_k C_b} We_i \right) \cos(\omega t) + \frac{1}{\omega} \left(\frac{dy_0}{dt} + \frac{y_0 - \frac{C_F}{C_k C_b} We_i}{t_d} \right) \sin(\omega t) \right). \quad (4)$$

The values of ω and t_d are computed from

$$\frac{1}{t_d} = \frac{C_d}{2} \frac{\mu_l}{\rho_l L^2}, \\ \omega^2 = C_k \frac{\sigma}{\rho_l L^3} - \frac{1}{t_d^2},$$

and We_i is the Weber number for particle i . It is calculated as follows:

$$We_i = \frac{\rho_a v_{i,rel}^2 L}{\sigma}.$$

We set both y_0 and $\frac{dy_0}{dt}$ in Eq. (4) to 0, as it is done in [OA87]. This allows to simplify Eq. (4):

$$y_i(t) = \frac{C_F}{C_k C_b} We_i \left(1 - e^{-\frac{t}{t_d}} \left(\cos(\omega t) + \frac{1}{\omega t_d} \sin(\omega t) \right) \right). \quad (5)$$

Next, we make the simplifying assumption that the particle is always deformed as strongly as possible according to Eq. (3). We find this maximum deformation by calculating the maximum of Eq. (5). We compute its derivative, set it equal to zero and solve the resulting equation. Accordingly, the maximum deformation is at time t^{\max} :

$$t^{\max} = -2 \frac{\tan^{-1} \left(\sqrt{t_d^2 \omega^2 + t_d} \right) - \pi}{\omega}. \quad (6)$$

Equation (6) only contains values that are independent of the liquid particle i . This allows us to precompute t^{\max} once and use it for all particles of the liquid, further saving computation time.

By inserting Eq. (6) into Eq. (5), we compute the maximum de-

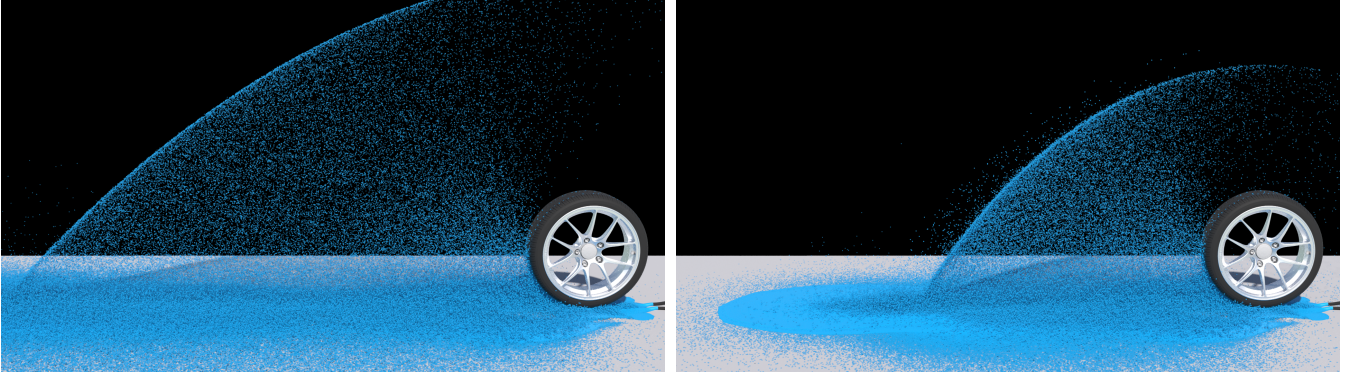


Figure 2: A wheel rotating with a speed corresponding to 20kmh^{-1} . When not using our drag force (left), the particles are sprayed very far. Applying our drag force (right), the particles reach a terminal velocity and the spray distance matches real-world experiments.

formation y_i^{\max} of particle i :

$$y_i^{\max} = \frac{C_F}{C_k C_b} W e_i \underbrace{\left(1 - e^{-\frac{t_i^{\max}}{\tau_d}} \left(\cos(\omega t_i^{\max}) + \frac{1}{\omega \tau_d} \sin(\omega t_i^{\max}) \right) \right)}_{=: c_{\text{def}}} \quad (7)$$

We show that everything in Eq. (7) apart from the relative velocity difference between particle i and surrounding air can be pre-computed and shared for all fluid particles to save computational cost:

$$\begin{aligned} y_i^{\max} &= \frac{C_F}{C_k C_b} \frac{\rho_a \mathbf{v}_{i,\text{rel}}^2 L}{\sigma} c_{\text{def}} \\ &= \mathbf{v}_{i,\text{rel}}^2 \underbrace{\frac{C_F}{C_k C_b} \frac{\rho_a L}{\sigma}}_{=: y_{\text{coeff}}} c_{\text{def}} \\ &= \mathbf{v}_{i,\text{rel}}^2 y_{\text{coeff}}. \end{aligned} \quad (8)$$

After pre-computing y_{coeff} , Eq. (8) allows to compute the current deformation of a particle with a single multiplication. In [OA87], if a droplet reaches a deformation of 1, it is assumed to break up into multiple smaller droplets. Since one particle is the smallest discretization unit in our SPH simulation, we clamp values larger than 1.

4.2. Drag Coefficient

Based on the deformation formula in [OA87], Liu et al. [LMR93] propose a model to compute the drag coefficient of a droplet. The idea is to use the deformation y to linearly interpolate the drag coefficient between the value of a sphere and the value of a disk. We adapt the formula from [LMR93] to use our calculated maximum deformation y_i^{\max} instead of the current deformation $y_i(t)$. The drag coefficient is then computed as:

$$C_{D,i}^{\text{Liu}} = C_{D,i}^{\text{sphere}} (1 + 2.632 y_i^{\max}), \quad (9)$$

where $C_{D,i}^{\text{sphere}}$ is the drag coefficient of a sphere. It is calculated as:

$$C_{D,i}^{\text{sphere}} = \begin{cases} \frac{24}{Re_i} \left(1 + \frac{1}{6} Re_i^{\frac{2}{3}} \right), & Re_i \leq 1000 \\ 0.424, & Re_i > 1000 \end{cases}$$

Re_i is the Reynolds number for particle i , which is computed as:

$$Re_i = \frac{\rho_a |\mathbf{v}_{i,\text{rel}}| L}{\mu_a}.$$

Finally, as we want a fluid particle which is part of a larger cluster of particles to have a drag coefficient of 1, we linearly interpolate between Eq. (9) and 1 based on the number of fluid neighbors n :

$$C_{D,i} = \left(1 - \frac{\min\left(\frac{2}{3} n^{\text{full}}, n\right)}{\frac{2}{3} n^{\text{full}}} \right) C_{D,i}^{\text{Liu}} + \frac{\min\left(\frac{2}{3} n^{\text{full}}, n\right)}{\frac{2}{3} n^{\text{full}}}. \quad (10)$$

n^{full} is the number of neighbors a particle with a full neighborhood has. If a particle has $\frac{2}{3} n^{\text{full}}$ neighbors, we assume it is part of a larger surface. In this case, its drag coefficient is 1. With no neighbors, the drag coefficient $C_{D,i}^{\text{Liu}}$ from Eq. (9) is used.

4.3. Particle Area

In this subsection, we explain how we compute the cross-sectional area of a deformed particle. Together with the occlusion detailed in the next subsection, this results in the area A_i used in the drag equation.

In SPH, the volume of a single particle is normally computed as the cube of the spacing h : $V_i = h^3$. This suggest to use the squared spacing as cross-sectional area of a particle:

$$A_i^{\text{square}} = h^2. \quad (11)$$

If the considered particle is part of a closed surface of a larger fluid volume, the particles arrange in layout with a distance of spacing to each other. Using the squared spacing as area fits well. When a fluid particle has no or only a few neighboring particles, this assumption is bad. A single fluid droplet forms a sphere as long as no external forces act on it. This is due to the surface tension. If a surface force like the drag force acts on a droplet, the droplet deforms

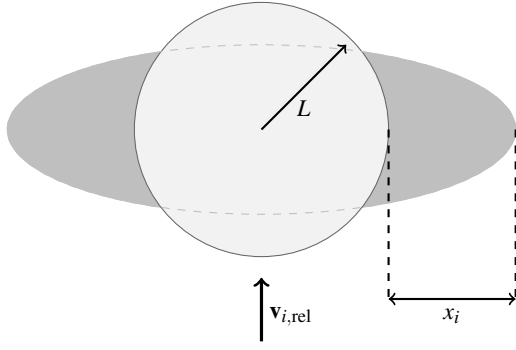


Figure 3: Illustration of the deformation of a single particle due to its relative velocity difference to the surrounding air $\mathbf{v}_{i,\text{rel}}$.

and more resembles a disk than a sphere (see Fig. 3). To compute the correct cross-sectional area for these particles, we again use the deformation value y_i^{max} computed in Subsection 4.1.

The cross-sectional area of a spherical droplet with radius L is computed as $A^{\text{sphere}} = \pi L^2$. Following [LMR93], the radius increase of a deformed droplet is calculated as:

$$y_i^{\text{max}} = \frac{x_i}{C_b L}$$

$$\implies x_i = C_b L y_i^{\text{max}}.$$

The radius of the deformed droplet is then $L + C_b L y_i^{\text{max}}$. This results in the following cross-sectional area of the disk-like droplet:

$$A_i^{\text{droplet}} = \pi (L + C_b L y_i^{\text{max}})^2. \quad (12)$$

Finally, we linearly interpolate between Eq. (11) and Eq. (12) based on the number of neighbors n . Similar to Eq. (10), with $\frac{2}{3}n^{\text{full}}$ neighbors, the area corresponds to the square area, while with no neighbors we use A_i^{droplet} . This results in the cross-sectional area of a particle:

$$A_i^{\text{unoccluded}} = \left(1 - \frac{\min\left(\frac{2}{3}n^{\text{full}}, n\right)}{\frac{2}{3}n^{\text{full}}}\right) A_i^{\text{droplet}} + \frac{\min\left(\frac{2}{3}n^{\text{full}}, n\right)}{\frac{2}{3}n^{\text{full}}} h^2. \quad (13)$$

We marked the area as unoccluded since we get the final area A_i used in Eq. (2) by combining Eq. (13) with a scaling based on the occlusion of the particle. This is explained in the next subsection.

4.4. Particle Occlusion

The drag forces should only act on particles that are exposed to the air, i.e., particles that are on the surface of the liquid. Additionally, only particles with a surface area facing towards $\mathbf{v}_{i,\text{rel}}$ should be influenced. To compute the occluded surface area of a particle, we first calculate the unoccluded area $A_i^{\text{unoccluded}}$ as detailed in Subsection 4.3. This area is then weighted with an occlusion value w_i . The value is between 0 and 1 and states the fraction of the particle area that is occluded,

$$A_i = w_i A_i^{\text{unoccluded}}. \quad (14)$$

A surface detection algorithm is needed to compute w_i . One common approach to detect surface particles of an SPH fluid is to compute a color field [Mor00, MCG03]. Surface particles are detected based on the magnitude of the gradient of this color field, which can be interpreted as the normal of the fluid. We noticed that this approach works well to simply detect surface particles. In our case, we want to additionally compute the ratio of exposed surface area of a single particle in the direction of the relative velocity between the particle and the air. This allows us to partially apply the drag force on these particles. Using the fluid color gradient for this proved to be difficult. For droplets with only a few particles the normal direction tends to vary strongly depending on the particle configuration. Therefore, we use a more geometrically inspired approach to compute the surface particles and their occlusion. Our method is similar to the idea used in [BTN13] and [YLM*16].

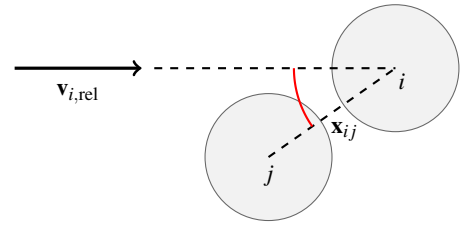


Figure 4: Computation of the occlusion is based on the angle between $\mathbf{v}_{i,\text{rel}}$ and the direction to neighboring particles \mathbf{x}_{ij} .

The algorithm in [BTN13] and [YLM*16] computes a cover vector \mathbf{b}_i and checks if there is a neighboring particle in a cone in the direction of this vector. If not, the particle is marked as being on the surface. We are interested in the occlusion in the direction of $\mathbf{v}_{i,\text{rel}}$ and therefore use this direction instead of the cover vector.

Furthermore, we do not declare a particle as fully covered or uncovered if it has a neighbor inside the scan cone. Instead, we use the cosine of the angle between $\mathbf{v}_{i,\text{rel}}$ and the neighbor direction \mathbf{x}_{ij} . For multiple neighbors, we use the maximum of this value. This results in a value between 0 and 1 which indicates the amount of occlusion of the particle. To get a value of 1 if the particles is not occluded at all, the occlusion value w_i for Eq. (14) is computed as.

$$w_i = 1 - \max_j \left(\frac{\mathbf{v}_{i,\text{rel}} \cdot \mathbf{x}_{ij}}{|\mathbf{v}_{i,\text{rel}}| |\mathbf{x}_{ij}|} \right). \quad (15)$$

To prevent values larger than 1 or smaller than 0, we additionally clamp w_i to this range.

4.5. Summary

Using the values from the previous subsections allows to compute Eq. (2). Algorithm 1 gives an overview over the order of steps.

The drag force is computed in the beginning of a simulation step since the drag force is added as external force. We require neighbor information for each particle to exist. Since these are necessary anyway for an SPH solver, this imposes no additional computational cost.

The only parameters required by the formulas in the algorithm are the surface tension and viscosity of the liquid as well as the rest

Algorithm 1 Drag force computation.

```

compute  $t_i^{\max}$  Eq. (6) and  $y_{\text{coeff}}$  Eq. (8)
for all particle  $i$  do
  compute deformation:  $y_i^{\max} = \mathbf{v}_{i,\text{rel}}^2 y_{\text{coeff}}$  using Eq. (8)
  compute drag coefficient  $C_{D,i}$  using Eq. (10)
  compute unoccluded area  $A_i^{\text{unoccluded}}$  using Eq. (13)
  compute occlusion  $w_i$  using Eq. (15)
  compute exposed area:  $A_i = w_i A_i^{\text{unoccluded}}$  using Eq. (14)
  compute drag force:  $\mathbf{F}_i^{\text{drag}} = \frac{1}{2} \rho_a \mathbf{v}_{i,\text{rel}}^2 C_{D,i} A_i$  using Eq. (2)

```

density of the air and the liquid. These values can be taken from literature.

5. Results

In this section, we show the properties of our drag force approach and demonstrate its effects on fluid behavior. In the presented experiments, we combine our force with different types of SPH solvers. Independent of the type of solver, we employ a cubic spline kernel [Mon05] with an influence radius of twice the particle spacing. Boundary handling with one-way and two-way coupling is implemented according to [AIA*12]. Surface tension is modeled with [AAT13].

The scenes are simulated on a 16-core Intel Xeon workstation with 3.1 GHz and 128 GB of RAM. Apart from the multiphase comparison and the wiper scene, which are rendered in our own SPH framework, the ray-traced images are rendered with [Sid]. If not noted otherwise, we use the drag force parameters shown in Section 4 and a constant air velocity of zero.

5.1. Comparison with Multiphase Simulation

Figure 1 shows the scenario we use to compare the visual effects resulting from our approach with a single-phase simulation without our approach and a full multiphase simulation. For all three simulations, IISPH [ICS*14] is used as a pressure solver. To improve the multiphase interactions, we employ a number-density-based formulation [SP08]. We set the density for the gas phase to 50 kg m^{-3} and for the liquid phase to 1000 kg m^{-3} . The particle spacing is 1 cm.

During the simulation, up to 100k liquid particles are emitted. For the multiphase simulation, there are an additional 2.7M air particles. Comparing the simulations illustrates that with our approach, a behavior similar to the multiphase simulation is achieved. Since no air particles are needed, the computation is significantly cheaper. Simulating 350 frames with one frame corresponding to 0.0001 s took 30 min for the multiphase simulation. Both single-phase simulations took 22 s.

5.2. Reaching of Terminal Velocity

Figure 5 shows a graph of the velocity profile of a single liquid particle that is accelerating due to a gravity of 9.81 m s^{-2} . The particle diameter is 5 mm. When only affected by the gravity, the particle accelerates indefinitely. Applying our proposed drag force, the particle reaches a terminal velocity when the gravity and drag force

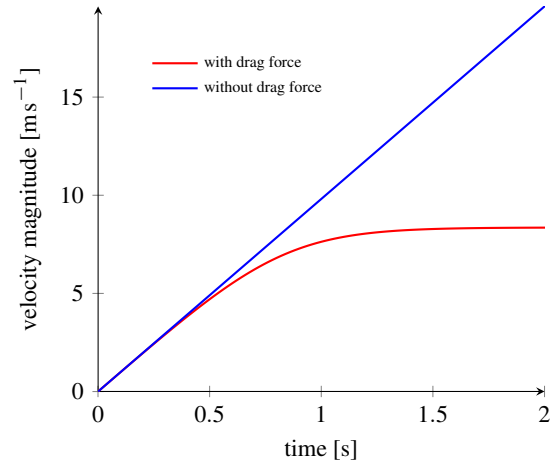


Figure 5: Velocity profile of a single particle with a diameter of 5 mm being accelerated due to gravity. When employing our drag force, the particle reaches a terminal velocity which matches the expected one.

cancel each other out. The terminal velocity of the particle affected by our drag force matches the values measured for falling raindrops of the same size [GK49, FDT69].

Particles reaching a terminal velocity is also an important property for more complex scenes. Figure 2 shows a tire testing setup: A wheel rotates on a large cylinder and water is flowing in from the right side. The rotation speed of the wheel corresponds to 20 km h^{-1} . Due to friction and adhesion between the water and the tire, the water is sprayed away from the tire. In this scene, the water is simulated with WCSPH [BT07] and the particle spacing is set to 1 mm. During the 8 s of simulated time, up to 3.2M particles are generated. Without our drag force, the particles do not reach a terminal velocity. In contrast, using our proposed drag force, the particles reach a terminal velocity and the spray distance is more plausible.

5.3. Combination with Different SPH Solvers

Since our force is added as an external force, it can be combined with different types of SPH solvers. First, we integrated our force into WCSPH [BT07] for the simulation of Fig. 2. The simulations in Figs. 1 and 7 use IISPH [ICS*14]. Additionally, we combined the drag force with an SPH solver for viscous fluids based on [PICT15]. The scene is shown in Fig. 6. A bunny is shot with a cannon ball made out of viscous fluid. The cannon ball consists of 800k particles with a particle spacing of 1 mm. It is shot with a speed of 10 m s^{-1} . The cannon ball deforms due to the drag forces acting on it. Since we compute an occlusion for each particle, the drag force only acts on the front of the cannon ball.

5.4. Coupling with Precomputed Air Flow

Figure 7 shows a wiper simulation. The scene contains a lot of animated, complex-shaped geometry. The liquid is simulated with IISPH [ICS*14] with a particle spacing of 1.25 mm. Up to 1.9M

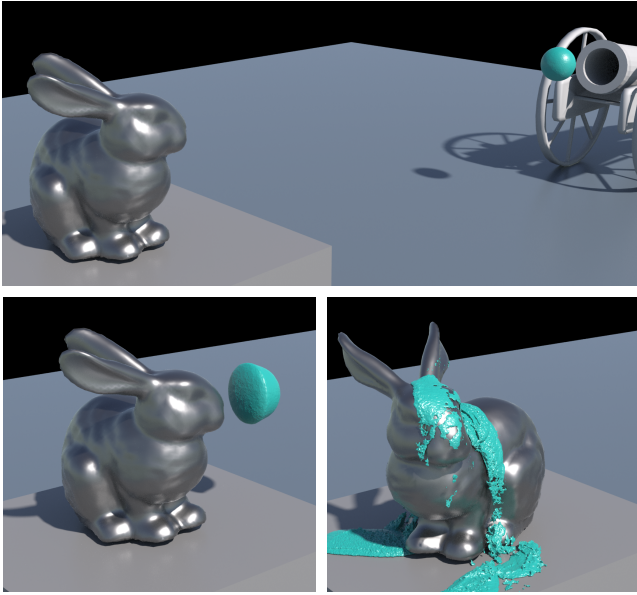


Figure 6: The Stanford Bunny being shot with a viscous cannon ball. The cannon ball consists of 800k fluid particles and deforms due to the drag force. The cannon model is courtesy of dberube4 on www.blendswap.com.

particles are simulated. Instead of assuming a constant air velocity everywhere, a grid of air velocities is imported from a previous aerodynamic simulation done with [Das]. This allows to take the air flow at the windshield apron and inside the motor compartment into account, which also influences the liquid flow. A comparison between the simulation with imported air velocities and a constant air velocity is shown in the accompanying video. It demonstrates that the air has a strong influence on the overall liquid behavior.

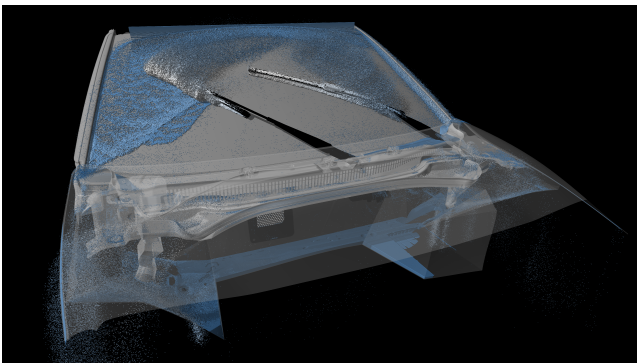


Figure 7: Wiper simulation. The air velocities used for the drag force have been precomputed with an aerodynamic simulation. This allows to consider complex air flows.

6. Conclusion

We presented a drag force formulation to model the effects of air onto an SPH free-surface liquid. Our proposed force takes the ex-

posed surface area of the liquid into account and models the deformation of particles.

We have shown that our force allows to capture effects acting from a second phase onto the liquid. We compared a simulation with our drag force to a multiphase simulation and showed matching results. Since with our approach the surrounding air does not need to be sampled with particles, it is computationally cheaper than a multiphase simulation. Since we add our drag force as an explicit force, it can be combined with different types of SPH solvers. We combine our force with different SPH pressure solvers and also with solvers for different materials. Multiple scenes have been simulated to show the effects of our drag force.

6.1. Limitations and Future Work

Depending on the resolution of the fluid, i.e., the size of a single particle, the terminal velocity of the particle varies. This can be problematic when the particle spacing is larger than a fluid droplet would be in reality. Furthermore, the radius used for the neighborhood search influences which particle contribute to the occlusion of particles. Since we set the neighborhood search radius depending on the particle spacing, this also varies with simulation resolution. This problem could be fixed by decoupling the neighborhood search radius for the occlusion computation from the SPH neighborhood. However, this may require more memory and computational effort.

With our approach, we cannot simulate entrapped air inside a liquid since we do not represent the air with particles. However, it is probably feasible to combine it with approaches that model these effects. Another possible improvement in this area could be to couple a coarse grid-based air simulation with the SPH liquid simulation using our proposed drag force.

Finally, we combined our drag force with an SPH solver capable of simulating deformable objects. For the solver implementation, we followed [Gan15]. [BIT09, SSP07] would also be possible choices. As shown in Fig. 8, it is possible to produce interesting effects, although it is hard to verify the realism of the results. An interesting future topic could be to try to simulate falling leaves to achieve results similar to the ones shown in [MUB15].

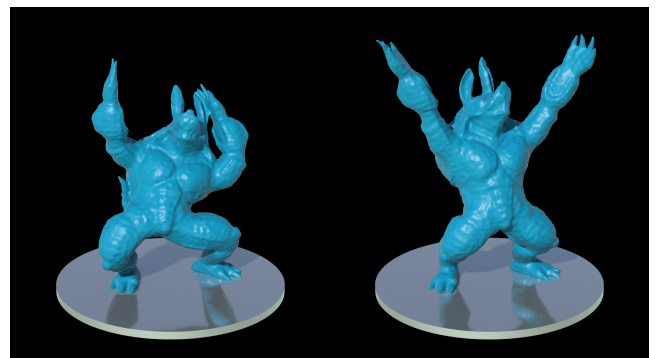


Figure 8: Armadillo dancing in the wind. The Armadillo is simulated as deformable object and consists of 230k SPH particles. The air velocity points upwards.

Acknowledgments

We would like to thank the reviewers for their helpful comments. This project is partially supported by the German Research Foundation (DFG) under contract number TE 632-1/2. The Armadillo and Bunny models are courtesy of the Stanford Computer Graphics Laboratory. We thank BBS Motorsport GmbH for providing the rim model for the tire testing scene. Further, we thank FIFTY2 Technology's team members for their support. We also want to give special thanks to Michael Ehlen from qpunkt GmbH for providing feedback and ideas.

References

- [AAT13] AKINCI N., AKINCI G., TESCHNER M.: Versatile Surface Tension and Adhesion for SPH Fluids. *ACM Trans. Graph.* 32, 6 (Nov. 2013), 182:1–182:8. 7
- [AIA*12] AKINCI N., IHMSEN M., AKINCI G., SOLENTHALER B., TESCHNER M.: Versatile Rigid-fluid Coupling for Incompressible SPH. *ACM Trans. Graph.* 31, 4 (July 2012), 62:1–62:8. 7
- [And01] ANDERSON JR. J. D.: *Fundamentals of Aerodynamics*, third ed. McGraw-Hill, 2001. 3
- [BIT09] BECKER M., IHMSEN M., TESCHNER M.: Corotated SPH for Deformable Solids. In *Proceedings of the Fifth Eurographics Conference on Natural Phenomena* (Aire-la-Ville, Switzerland, Switzerland, 2009), NPH'09, Eurographics Association, pp. 27–34. 8
- [BK17] BENDER J., KOSCHIER D.: Divergence-Free SPH for Incompressible and Viscous Fluids. *IEEE Transactions on Visualization and Computer Graphics* 23, 3 (Mar. 2017), 1193–1206. 3
- [BT07] BECKER M., TESCHNER M.: Weakly Compressible SPH for Free Surface Flows. In *Proceedings of the 2007 ACM SIGGRAPH/Eurographics Symposium on Computer Animation* (Aire-la-Ville, Switzerland, Switzerland, 2007), SCA '07, Eurographics Association, pp. 209–217. 3, 7
- [BTH*03] BHAT K. S., TWIGG C. D., HODGINS J. K., KHOSLA P. K., POPOVIĆ Z., SEITZ S. M.: Estimating Cloth Simulation Parameters from Video. In *Proceedings of the 2003 ACM SIGGRAPH/Eurographics Symposium on Computer Animation* (Aire-la-Ville, Switzerland, Switzerland, 2003), SCA '03, Eurographics Association, pp. 37–51. 3
- [BTN13] BARECASCO A., TERISSA H., NAA C. F.: Simple free-surface detection in two and three-dimensional SPH solver. *Selected Papers from the International Symposium on Computational Science Kanazawa University, Japan 4* (2013), 1–10. 6
- [CPPK07] CLEARY P. W., PYO S. H., PRAKASH M., KOO B. K.: Bubbling and Frothing Liquids. *ACM Trans. Graph.* 26, 3 (July 2007). 2, 3
- [Das] DASSAULT SYSTÈMES: XFlow. www.xflowcfd.com. 8
- [FDT69] FOOTE G. B., DU TOIT P. S.: Terminal Velocity of Raindrops Aloft. *Journal of Applied Meteorology* 8, 2 (1969), 249–253. 7
- [Gan15] GANZENMÜLLER G. C.: An hourglass control algorithm for Lagrangian Smooth Particle Hydrodynamics. *Computer Methods in Applied Mechanics and Engineering* 286 (2015), 87–106. 8
- [GK49] GUNN R., KINZER G. D.: The Terminal Velocity of Fall for Water Droplets in Stagnant Air. *Journal of Meteorology* 6, 4 (1949), 243–248. 7
- [HLYK08] HONG J.-M., LEE H.-Y., YOON J.-C., KIM C.-H.: Bubbles Alive. *ACM Trans. Graph.* 27, 3 (Aug. 2008), 48:1–48:4. 2
- [IAAT12] IHMSEN M., AKINCI N., AKINCI G., TESCHNER M.: Unified Spray, Foam and Air Bubbles for Particle-based Fluids. *Vis. Comput.* 28, 6-8 (June 2012), 669–677. 1
- [IBAT11] IHMSEN M., BADER J., AKINCI G., TESCHNER M.: Animation of Air Bubbles with SPH. In *GRAPP 2011 - Proceedings of the International Conference on Computer Graphics Theory and Applications, Vilamoura, Algarve, Portugal, March 5-7, 2011* (2011), pp. 225–234. 1, 2
- [ICS*14] IHMSEN M., CORNELIS J., SOLENTHALER B., HORVATH C., TESCHNER M.: Implicit Incompressible SPH. *IEEE Transactions on Visualization and Computer Graphics* 20, 3 (Mar. 2014), 426–435. 3, 7
- [IOS*14] IHMSEN M., ORTHMANN J., SOLENTHALER B., KOLB A., TESCHNER M.: SPH Fluids in Computer Graphics. In *Eurographics 2014 - State of the Art Reports* (2014), Lefebvre S., Spagnuolo M., (Eds.), The Eurographics Association. 1, 2
- [KKTW04] KECKEISEN M., KIMMERLE S., THOMASZEWSKI B., WACKER M.: Modelling Effects of Wind Fields in Cloth Animations. *Journal of WSCG* 12, 1–3 (2004). 3
- [LMR93] LIU A. B., MATHER D., REITZ R. D.: Modeling the Effects of Drop Drag and Breakup on Fuel Sprays. In *SAE Technical Paper* (Mar. 1993), SAE International. 5, 6
- [LSRS99] LOMBARDI J. C., SILLS A., RASIO F. A., SHAPIRO S. L.: Tests of Spurious Transport in Smoothed Particle Hydrodynamics. *Journal of Computational Physics* 152, 2 (July 1999), 687–735. 2
- [MCG03] MÜLLER M., CHARYPAR D., GROSS M.: Particle-based Fluid Simulation for Interactive Applications. In *Proceedings of the 2003 ACM SIGGRAPH/Eurographics Symposium on Computer Animation* (Aire-la-Ville, Switzerland, Switzerland, 2003), SCA '03, Eurographics Association, pp. 154–159. 2, 6
- [MFZ97] MORRIS J. P., FOX P. J., ZHU Y.: Modeling Low Reynolds Number Incompressible Flows Using SPH. *J. Comput. Phys.* 136, 1 (Sept. 1997), 214–226. 3
- [MMCK14] MACKLIN M., MÜLLER M., CHENTANEZ N., KIM T.-Y.: Unified Particle Physics for Real-time Applications. *ACM Trans. Graph.* 33, 4 (July 2014), 153:1–153:12. 1, 3
- [Mon05] MONAGHAN J. J.: Smoothed particle hydrodynamics. *Reports on Progress in Physics* 68, 8 (2005), 1703. 2, 7
- [Mor00] MORRIS J. P.: Simulating surface tension with smoothed particle hydrodynamics. *International Journal for Numerical Methods in Fluids* 33, 3 (2000), 333–353. 6
- [MSKG05] MÜLLER M., SOLENTHALER B., KEISER R., GROSS M.: Particle-based Fluid-fluid Interaction. In *Proceedings of the 2005 ACM SIGGRAPH/Eurographics Symposium on Computer Animation* (New York, NY, USA, 2005), SCA '05, ACM, pp. 237–244. 1, 2, 3
- [MUB15] MARTIN T., UMETANI N., BICKEL B.: OmniAD: Data-driven Omni-directional Aerodynamics. *ACM Trans. Graph.* 34, 4 (July 2015), 113:1–113:12. 8
- [NG72] NELSON A. R., GOKHALE N. R.: Oscillation Frequencies of Freely Suspended Water Drops. *Journal of Geophysical Research* 77, 15 (1972), 2724–2727. 4
- [OA87] O'ROURKE P. J., AMSDEN A. A.: The Tab Method for Numerical Calculation of Spray Droplet Breakup. In *SAE Technical Paper* (Nov. 1987), SAE International. 4, 5
- [PICT15] PEER A., IHMSEN M., CORNELIS J., TESCHNER M.: An Implicit Viscosity Formulation for SPH Fluids. *ACM Trans. Graph.* 34, 4 (July 2015), 114:1–114:10. 3, 7
- [SB12] SCHECHTER H., BRIDSON R.: Ghost SPH for Animating Water. *ACM Trans. Graph.* 31, 4 (July 2012), 61:1–61:8. 1, 3
- [Sid] SIDE EFFECTS SOFTWARE: Houdini. www.sidefx.com. 7
- [SP08] SOLENTHALER B., PAJAROLA R.: Density Contrast SPH Interfaces. In *Proceedings of the 2008 ACM SIGGRAPH/Eurographics Symposium on Computer Animation* (Aire-la-Ville, Switzerland, Switzerland, 2008), SCA '08, Eurographics Association, pp. 211–218. 2, 7
- [SP09] SOLENTHALER B., PAJAROLA R.: Predictive-corrective Incompressible SPH. *ACM Trans. Graph.* 28, 3 (July 2009), 40:1–40:6. 3

- [SSP07] SOLENTHALER B., SCHLÄFLI J., PAJAROLA R.: A unified particle model for fluid-solid interactions. *Computer Animation and Virtual Worlds* 18, 1 (2007), 69–82. [8](#)
- [Tay63] TAYLOR G. I.: The Shape and Acceleration of a Drop in a High Speed Air Stream. *The Scientific Papers of Geoffrey Ingram Taylor* 3 (1963), 457–464. [4](#)
- [TDF*15] TAKAHASHI T., DOBASHI Y., FUJISHIRO I., NISHITA T., LIN M. C.: Implicit Formulation for SPH-based Viscous Fluids. *Comput. Graph. Forum* 34, 2 (May 2015), 493–502. [3](#)
- [TM05] TARTAKOVSKY A. M., MEAKIN P.: A Smoothed Particle Hydrodynamics Model for Miscible Flow in Three-dimensional Fractures and the Two-dimensional Rayleigh-Taylor Instability. *J. Comput. Phys.* 207, 2 (Aug. 2005), 610–624. [2](#)
- [VM12] VOLLMER M., MÖLLMANN K.-P.: Oscillating droplets and incompressible liquids: slow-motion visualization of experiments with fluids. *Physics Education* 47, 6 (2012), 664. [4](#)
- [WMLS14] WILSON K., MCADAMS A., LEO H., SIMMONS M.: Simulating Wind Effects on Cloth and Hair in Disney’s Frozen. In *ACM SIGGRAPH 2014 Talks* (New York, NY, USA, 2014), SIGGRAPH ’14, ACM, pp. 48:1–48:1. [3](#)
- [YLM*16] YANG T., LIN M. C., MARTIN R. R., CHANG J., HU S.-M.: Versatile Interactions at Interfaces for SPH-based Simulations. In *Proceedings of the ACM SIGGRAPH/Eurographics Symposium on Computer Animation* (Aire-la-Ville, Switzerland, Switzerland, 2016), SCA ’16, Eurographics Association, pp. 57–66. [6](#)